

Multi-frequency non-reciprocal optical directional amplifier realized with non-Hermitian resonator arrays

Jin-Xiang Xue(薛金香), Chuan-Xun Du(杜传勋), Cheng-Chao Liu(刘成超), Liu Yang(杨柳), and Yong-Long Wang(王永龙)

Citation: Chin. Phys. B, 2026, 35 (**2**): 024207. DOI: 10.1088/1674-1056/adf69d
http://cpb.iphy.ac.cn; http://iopscience.iop.org/cpb

What follows is a list of articles you may be interested in

Theoretical and computational feasibility of femtosecond laser multifilament transverse structures reconstruction via circular-scanning-based photoacoustic tomography

Qingwei Zeng(曾庆伟), Lei Liu(刘磊), Shuai Hu(胡帅), and Shulei Li(李书磊)
Chin. Phys. B, 2025, 34 (**9**): 094209. DOI: 10.1088/1674-1056/ade663

Synchronized dual-wavelength mode-locked laser in normal dispersion regime

Yangrui Shi(史洋瑞), Haojing Zhang(张皓景), Yuxuan Ren(任俞宣), Junsong Peng(彭俊松), and Heping Zeng(曾和平)
Chin. Phys. B, 2025, 34 (**9**): 094207. DOI: 10.1088/1674-1056/add4fe

Strain modulation of second harmonic generation in new tetrahedral transition metal dichalcogenide monolayers

Hu Chen(陈虎), Shi-Qi Li(李仕琪), Yuqing Wu(吴雨晴), Xiaozhendong Bao(鲍晓振东), Zhijie Lei(雷志杰), Hongsheng Liu(柳洪盛), Yuee Xie(谢月娥), Junfeng Gao(高峻峰), Yuanping Chen(陈元平), and Xiaohong Yan(颜晓红)
Chin. Phys. B, 2025, 34 (**8**): 084206. DOI: 10.1088/1674-1056/addaa3

Simultaneous second and third harmonics generation in periodically poled lithium niobate: Coupling and competition

Junming Liu(刘峻铭), Liqiang Liu(刘励强), Lihong Hong(洪丽红), and Zhiyuan Li(李志远)
Chin. Phys. B, 2025, 34 (**8**): 084203. DOI: 10.1088/1674-1056/add24a

Anti-$\mathcal{PT}$-symmetric Kerr gyroscope

Huilai Zhang(张会来), Meiyu Peng(彭美瑜), Xun-Wei Xu(徐勋卫), and Hui Jing(景辉)
Chin. Phys. B, 2022, 31 (**1**): 014215. DOI: 10.1088/1674-1056/ac3988

Multi-frequency non-reciprocal optical directional amplifier realized with non-Hermitian resonator arrays

Jin-Xiang Xue(薛金香)[1], Chuan-Xun Du(杜传勋)[1,3,†], Cheng-Chao Liu(刘成超)[1], Liu Yang(杨柳)[1], and Yong-Long Wang(王永龙)[1,2,3,‡]

[1] *School of Physics and Electronic Engineering, Linyi University, Linyi* 276005, *China*
[2] *Department of Physics, Nanjing University, Nanjing* 210093, *China*
[3] *National Laboratory of Solid State Microstructures, Nanjing University, Nanjing* 210093, *China*

(Received 14 April 2025; revised manuscript received 30 July 2025; accepted manuscript online 1 August 2025)

For a multi-frequency non-reciprocal optical device, we first realize multi-frequency optical non-reciprocal transmission using a non-Hermitian multi-mode resonator array. Practically, multi-frequency operation can add channels to the non-reciprocal optical device and the non-reciprocity can route optical signals and prevent the reverse flow of noise. Using the Scully–Lamb model and gain saturation effect, we accomplish dual-frequency non-reciprocal transmission by introducing nonlinearity into a linear array of four-mode resonators. The accomplishment is directly demonstrated by the non-reciprocal transmission phenomena present in the non-divergent peaks. For example, a directional cyclic amplifier is constructed with non-reciprocal units. Regarding potential applications, non-reciprocal optical systems can be employed in dual-frequency control, parallel information processing, photonic integrated circuits, optical devices and so on.

Keywords: non-Hermitian systems, $\mathcal{PT}$-symmetry, multi-frequency of non-reciprocity, optical directional amplifier

PACS: 42.65.–k, 42.50.Pq, 03.65.Yz

DOI: 10.1088/1674-1056/adf69d **CSTR:** 32038.14.CPB.adf69d

1. Introduction

For a long time, optical devices have been widely studied in optical communication, optical imaging, optical sensing and so on.[1,2] Recently, the non-reciprocal optical phenomenon was investigated for the unidirectional flow of light, which is essential for preventing backscattering and enhancing signal integrity. The realization of unidirectional amplifiers and circulators has made it possible to construct advanced photonic systems that can efficiently manage optical signals.[3] Although previous studies, such as those referenced in Ref. [4], have successfully demonstrated optical unidirectional amplifiers and circulators, these implementations often rely on magnetic fields, which complicates integration into compact photonic circuits. To address this limitation, the phenomena of non-reciprocity in optical cavities discussed in Refs. [5,6] offer a promising route. In this work, we first extend the single-frequency non-reciprocal system discussed in Ref. [5] to a multi-frequency system, enhancing its capability for parallel information processing. We then propose an initial design for a unidirectional amplifier utilizing non-reciprocal optical cavities for more complex and integrated photonic devices.

The reciprocity of an optical system means that the response of the system does not change when a light wave is back-propagated along the direction of propagation.[7] This feature is valuable in many optical systems and devices. However, non-reciprocity plays a more important role in optical devices; this occurs when the intensity of propagating light waves is considerably differently in the forward and backward directions.[8–10] Non-reciprocity is important in photonic information processing to route optical signals or prevent the reverse flow of noise. Non-reciprocity is employed in optical devices[11–14] in which the interference effect would be effectively reduced to protect the signal source from noise interference. As a result, non-reciprocal optical devices are more accurate and reliable, which is of great significance for research into communication technology,[15,16] information processing,[13,17] precision measurement[12,18] and topological photonics.[19,20] Various non-reciprocal devices have been realized for single-frequency applications,[3,21–23] but these is still a need to improve the multi-channel information processing capability of non-reciprocal optical devices, especially those that can be easily integrated into optical chips.[24] Non-reciprocity can be generated through various methods,[25–29] including the application of a magnetic field,[30,31] dynamic modulation of the dielectric constant,[30,32,33] optical nonlinearity,[17,34–36] and so on. In terms of dynamic modulation permittivity and optical nonlinearity, non-reciprocal mechanisms were applied to superconducting microwave circuits.[21,37–41] For potential ap-

†Corresponding author. E-mail: duchuanxun@lyu.edu.cn
‡Corresponding author. E-mail: wangyonglong@lyu.edu.cn

© 2026 Chinese Physical Society and IOP Publishing Ltd. All rights, including for text and data mining, AI training, and similar technologies, are reserved.

plications, the first considerations should be integration, stability and controllability. In the absence of a magnetic field these aspects become more difficult. However, high integration, strong stability and good controllability can be easily achieved in optical devices by using the optical nonlinear effect.[18] For a parity–time symmetric photonic device consisting of two resonators,[5] light propagation was analyzed by the non-Lindbladian master equation of the Scully–Lamb laser model. By semi-classical approximation, two nonlinear coupled differential equations were obtained for the field evolution in a cavity, which explained the non-reciprocity[42] and demonstrated that the gain saturation effect is the key mechanism of non-reciprocity.[5] It is worth noting that the known non-reciprocity phenomenon mostly appears at the non-divergent peak of a single frequency. In our previous work,[43] a series of $\mathcal{PT}$-symmetric one-dimensional multimode resonator arrays were built and the transmission spectra discussed. In that system, non-reciprocity could be achieved by the gain saturation effect. We have replaced the transition point of the $\mathcal{PT}$ unbroken phase by that of broken phase in the parameter space, and have realized multiple non-divergent peaks in the transmission spectrum. Our results may provide a way to design multi-frequency non-reciprocal devices.

In the present paper, we aim to construct a dual-frequency non-reciprocal optical system with a non-Hermitian multi-mode resonator array. In terms of the Scully–Lamb model, we will give a nonlinear equation by introducing a nonlinear term into the original linear equation. With the gain saturation effect[5] and the non-Hermitian resonator array model, the known two-mode resonator system can be extended to a four-mode one. Then optical non-reciprocity of two frequencies can be achieved. This phenomenon can be applied to photodiodes, but also the dual-frequency non-reciprocity phenomenon and the parallel processing of multiple information. The system can be used to construct a multi-mode optical directional amplifier and isolators.[41,44–46] The amplifier with four ports is cascaded by the structure shown in Fig. 1, which consists of two optical fibers coupled to a series of silicon dioxide microring resonators. The signal can be input from one port, the output signal can be detected from the others, and the signal will be amplified with different times for different output ports. If only two ports are taken, the function of the isolator can be realized. The function of a directional amplifier can be realized by controlling the frequency mismatch between the input light and the cavity resonance. Compared with other directional amplifiers, this system has several advantages, such as dual-frequency control, circulability and easy integration.

The paper is organized as follows. In Section 2, the basic model and the linear dynamics equations are briefly introduced. In Section 3, the theoretical basis of the system is given and dual-frequency non-reciprocal transmission is achieved by a four-mode resonator system due to the presence of nonlinear gain saturation. In Section 4, a non-reciprocal double-frequency system is constructed and investigated. In Section 5, conclusions and discussions are given.

2. Basic model and linear dynamic equation

In this section a ring resonator array will be considered as the basic model and its linear dynamic equations will be discussed. With the linear equations, the positions and types of resonance peaks can be determined. For the Scully–Lamb model, by introducing nonlinear terms the nonlinear model can give rise to non-reciprocal transmission phenomena. The result plays an important role in the present paper. Specifically, the nonlinear terms introduced into the model can be taken as fundamental elements for constructing complex multi-mode non-reciprocal transmission systems and subsequent multi-mode unidirectional amplifiers.

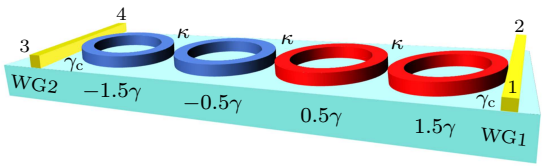


Fig. 1. A four-mode resonator array with balanced gain and loss. The resonators are coupled adjacent to each other with coupling strength κ. The coupling loss between waveguide WG1 (WG2) and resonator R_1 (R_4) is γ_c.

The considered system is a linear array of four coupled resonators depicted in Fig. 1. The non-reciprocal phenomenon in ring resonator arrays has been experimentally demonstrated in Ref. [42]. In terms of experimental preparation, the passive resonators, which are lossy, can be crafted from silica, while the active resonators, which provide gain, can be made from a silica film doped with erbium ions. This film is fabricated by the sol–gel technique, where the solution is prepared by blending tetraethoxysilane with isopropyl alcohol, water and hydrochloric acid. A reasonable theoretical extension was proposed on the basis of the above-mentioned experimental scheme. Compared with the work in Ref. [42], it is significant that there is an extension from a two-mode to a multi-mode configuration. The resonators have the same resonating frequency ω_0, and their couplings just occur between adjacent resonators with the same coupling strength that can be described by the real-valued parameter κ. The net gain or loss for the ith resonator can be encapsulated in a single parameter γ_i, where gain is indicated by $\gamma_i > 0$ and loss by $\gamma_i < 0$. Theoretically, we can adjust the above parameters to make the net gain or loss coefficient γ_i take any value. In the model discussed in this article, we let the gain–loss coefficient be arranged in an arithmetic sequence, as shown in Fig. 1. The probe signal is introduced through port 1 and the resulting signal can be monitored at port 4. The coupling strength between

the first resonator and the input signal's driving field, characterized by power P and frequency $\omega_{\rm in}$, is represented by ϵ, with the relationship defined as $\epsilon \equiv \sqrt{\gamma_{\rm c} P/\hbar\omega_{\rm in}}$.

When the input power P does not surpass the threshold for gain saturation effects,[47] and as long as the resonator peaks remain bounded, the gain within the active cavity behaves linearly. As a consequence, the dynamics of the optical field can be expressed as a set of linear equations[5,6,42]

$$\begin{aligned}
\frac{\rm d}{{\rm d}t}a_1 &= -{\rm i}\omega_0 a_1 + 1.5\gamma a_1 - {\rm i}\kappa a_2 - \epsilon\exp(-{\rm i}\omega_{\rm in}t),\\
\frac{\rm d}{{\rm d}t}a_2 &= -{\rm i}\omega_0 a_2 + 0.5\gamma a_2 - {\rm i}\kappa a_1 - {\rm i}\kappa a_3,\\
\frac{\rm d}{{\rm d}t}a_3 &= -{\rm i}\omega_0 a_3 - 0.5\gamma a_3 - {\rm i}\kappa a_2 - {\rm i}\kappa a_4,\\
\frac{\rm d}{{\rm d}t}a_4 &= -{\rm i}\omega_0 a_4 - 1.5\gamma a_4 - {\rm i}\kappa a_3.
\end{aligned} \tag{1}$$

By substituting $a_n = A_n\exp(-{\rm i}\omega_{\rm in}t)$ into Eq. (1), the dynamical equations for the field amplitude can be obtained as

$$\begin{aligned}
\frac{\rm d}{{\rm d}t}A_1 &= {\rm i}\Delta_{\rm in}A_1 + 1.5\gamma A_1 - {\rm i}\kappa A_2 - \varepsilon,\\
\frac{\rm d}{{\rm d}t}A_2 &= {\rm i}\Delta_{\rm in}A_2 + 0.5\gamma A_2 - {\rm i}\kappa A_1 - {\rm i}\kappa A_3,\\
\frac{\rm d}{{\rm d}t}A_3 &= {\rm i}\Delta_{\rm in}A_3 - 0.5\gamma A_3 - {\rm i}\kappa A_2 - {\rm i}\kappa A_4,\\
\frac{\rm d}{{\rm d}t}A_4 &= {\rm i}\Delta_{\rm in}A_4 - 1.5\gamma A_4 - {\rm i}\kappa A_3,
\end{aligned} \tag{2}$$

where $\Delta_{\rm in} = \omega_{\rm in} - \omega_0$ is the frequency-detuning parameter. In the steady state ${\rm d}A_n/{\rm d}t = 0$, one can obtain from Eq. (2) a series of linear equations as below:

$$\begin{cases}
{\rm i}\Delta_{\rm in}A_1 + 1.5\gamma A_1 - {\rm i}\kappa A_2 = \varepsilon,\\
{\rm i}\Delta_{\rm in}A_2 + 0.5\gamma A_2 - {\rm i}\kappa A_1 - {\rm i}\kappa A_3 = 0,\\
{\rm i}\Delta_{\rm in}A_3 - 0.5\gamma A_3 - {\rm i}\kappa A_2 - {\rm i}\kappa A_4 = 0,\\
{\rm i}\Delta_{\rm in}A_4 - 1.5\gamma A_4 - {\rm i}\kappa A_3 = 0.
\end{cases} \tag{3}$$

It is apparent that A_4 can be finally given by solving Eq. (3). In the semiclassical approximation, the coupling constant ϵ can be expressed via the amplitude $A_{\rm in}$ of the input driving field as $\epsilon \equiv \sqrt{\gamma_{\rm c}}A_{\rm in}$.[5] Then the transmission spectrum can be calculated by

$$T(\Delta_{\rm in}) = \left|\frac{A_{\rm out}}{A_{\rm in}}\right|^2, \tag{4}$$

where $A_{\rm out} = \sqrt{\gamma_{\rm c}}A_4$ and $A_{\rm in} = \epsilon/\sqrt{\gamma_{\rm c}}$. It is easy to check that when the parameter settings of γ and κ change, the distribution of resonant peaks on the graph of $T(\Delta_{\rm in})$ will become different. To study how non-reciprocity occurs on these peaks, one can rewrite Eqs. (2) and (3) in matrix form.

By defining a vector $\boldsymbol{\alpha} = (A_1, A_2, A_3, A_4)^{\rm T}$ with elements being the field amplitudes, and by introducing $\boldsymbol{\beta} = (\epsilon, 0, 0, 0)^{\rm T}$ describing the input condition, we can rewrite Eq. (2) in the form ${\rm i}\,{\rm d}A_n/{\rm d}t = \hat{\boldsymbol{H}}_4\boldsymbol{\alpha} - \boldsymbol{\beta}$, where the coefficient matrix $\hat{\boldsymbol{H}}_4$ reads

$$\hat{\boldsymbol{H}}_4 = \begin{pmatrix}
\Delta_{\rm in} + {\rm i}1.5\gamma & \kappa & 0 & 0\\
\kappa & \Delta_{\rm in} + {\rm i}0.5\gamma & \kappa & 0\\
0 & \kappa & \Delta_{\rm in} - {\rm i}0.5\gamma & \kappa\\
0 & 0 & \kappa & \Delta_{\rm in} - {\rm i}1.5\gamma
\end{pmatrix}, \tag{5}$$

which is known as the Hamiltonian or evolution matrix.[5,6,42] With $\boldsymbol{\alpha}$, $\boldsymbol{\beta}$ and $\hat{\boldsymbol{H}}_4$, Eq. (3) can be simplified as $\hat{\boldsymbol{H}}_4\boldsymbol{\alpha} = \boldsymbol{\beta}$, and then the steady-state solution of $\boldsymbol{\alpha}$ can be given by $\boldsymbol{\alpha} = \hat{\boldsymbol{H}}_4^{-1}\boldsymbol{\beta}$. For a particular set of γ and κ, the frequencies are indicative of the divergent peaks in the transmission spectrum, which are termed supermodes. The supermodes of the photon frequencies might be complex due to solutions involving imaginary parts. In what follows, for the sake of reality the series of non-divergent peaks will correspond to the real parts of these supermodes. Thus, the issue of resonant peaks is reduced to an eigenvalue problem.

In practice, the light intensity cannot be infinitely amplified. Actually, the divergent peaks should be replaced by a series of sharp but finite peaks. Intriguingly, non-reciprocal transmission phenomena emerge at non-divergent peaks.[42] This discovery has inspired physicists to investigate the underlying mechanisms. A plausible theory, the gain saturation theory, was put forward by Arkhipov's group.[5] In that theory, the nonlinear equations are derived from the Scully–Lamb laser model. It is worth noting that the nonlinear equations combine the simplicity of the linear model with the accuracy of the nonlinear model.

According to Ref. [5], the modification of the Scully–Lamb model to linear equations can be accomplished by adding a nonlinear term to each gain term. Upon examining the numerical outcomes of the dual-mode $\mathcal{PT}$ system (see Appendix A), two key insights emerge: one is the prediction of non-reciprocal peaks by the nonlinear equations; the other is the manifestation of non-reciprocal peaks within the non-divergent peaks region of $\mathcal{PT}$ symmetry breaking. Like the conclusion obtained in Ref. [43], the location of non-divergent peaks aligns with the projection of supermodes onto the real axis in the complex plane. This also means that by skillfully adjusting the parameters of the multi-mode system we can obtain multiple non-reciprocal peaks at different frequencies in the $\mathcal{PT}$ symmetry breaking region. This is the basis for the parameter settings when constructing the system shown in Fig. 1.

By numerically solving the secular equation, the supermodes $\Delta_{\rm r}$ of H are obtained; the real and imaginary parts of $\Delta_{\rm r}$ are described in Figs. 2(a) and 2(b). In region I (III), where γ is small (large), the supermodes $\Delta_{\rm r}$ are purely real (imaginary), while in region II, the real parts and imaginary parts of $\Delta_{\rm r}$ are all non-zero. In other words, the parameter space is divided into three regions: in region I, with $\mathcal{PT}$ unbroken, $\Delta_{\rm r}$ is real;

in region II, being the transition region, $\Delta_{\rm r}$ is complex; and in region III, with $\mathcal{PT}$ broken, $\Delta_{\rm r}$ is imaginary. In different regions the transmission spectrum has different behaviors, as shown in Fig. 2(c). In region I, the number of divergent peaks equals that of the supermodes, and in region III there is a single non-divergent peak on $\Delta_{\rm in}=0$. However, in region II, there is more than one non-divergent peak in the spectrum. Comparing Figs. 2(a) and 2(b), we find that the locations of non-divergent peaks coincide with the projections of supermodes onto the real axis. Based on the previous speculation, the multiple non-divergent peaks may successfully appear in region II.

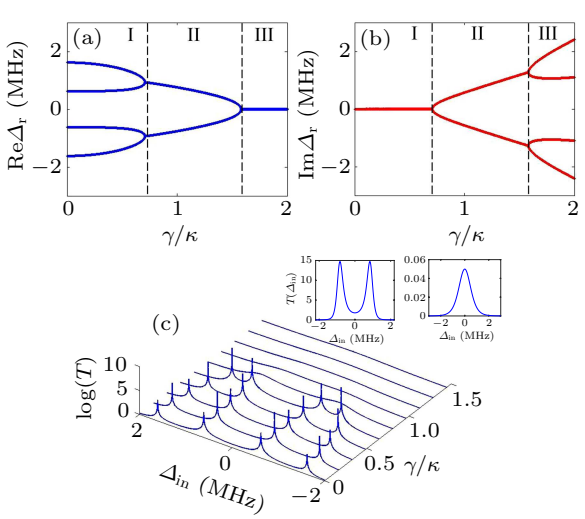


Fig. 2. (a) The real and (b) the imaginary parts of supermodes of $\hat{H}_4$ as functions of γ/κ. (c) Variation of the transmission spectrum as a function of γ/κ and $\Delta_{\rm in}$, where the logarithm of $T(\omega_l)$ is shown as the the perpendicular axis value. The insets show the transmission spectrum against $\Delta_{\rm in}$ of broken $\mathcal{PT}$ symmetry for two typical parameter values in region II ($\gamma=0.8$ MHz) and region III ($\gamma=1.8$ MHz).

3. Gain saturation effect and multi-mode non-reciprocal transmission

The active resonator essentially functions as a laser system incorporating a laser gain medium. To elucidate the dynamics of the electromagnetic field within the active laser resonator it is imperative to invoke the principles of quantum laser theory, specifically the master equation. In line with the analysis presented in Ref. [47], we shall regard our system as an ideal laser system within the Scully–Lamb laser model framework. This model is characterized by a non-Lindbladian master equation, which is particularly noteworthy due to its deviation from the conventional Lindbladian form. The non-Lindbladian nature of the master equation implies that the system's evolution may not strictly adhere to the standard dissipative processes typically described by Lindblad operators, thus potentially allowing for unique dynamical behaviors and quantum effects that merit further investigation. The non-Lindbladian master equation for the density operator $\hat{\rho}$ of the optical fields can be formulated as follows:

$$\begin{aligned}\frac{\mathrm{d}}{\mathrm{d}t}\hat{\rho} =& \frac{1}{\mathrm{i}\hbar}[\hat{H},\hat{\rho}]+\Big[\frac{A}{2}\left(\hat{a}_1^\dagger\hat{\rho}\hat{a}_1-\hat{a}_1\hat{a}_1^\dagger\hat{\rho}+\hat{a}_2^\dagger\hat{\rho}\hat{a}_2-\hat{a}_2\hat{a}_2^\dagger\hat{\rho}\right)\\&+\frac{B}{8}\left(\hat{\rho}\left(\hat{a}_1\hat{a}_1^\dagger\right)^2+3\hat{a}_1\hat{a}_1^\dagger\hat{\rho}\hat{a}_1\hat{a}_1^\dagger-4\hat{a}_1^\dagger\hat{\rho}\hat{a}_1\hat{a}_1^\dagger\hat{a}_1\right.\\&\left.+\hat{\rho}\left(\hat{a}_2\hat{a}_2^\dagger\right)^2+3\hat{a}_2\hat{a}_2^\dagger\hat{\rho}\hat{a}_2\hat{a}_2^\dagger-4\hat{a}_2^\dagger\hat{\rho}\hat{a}_2\hat{a}_2^\dagger\hat{a}_2\right)\\&+\sum_{i=1}^{4}\frac{\Gamma_i}{2}\left(\hat{a}_i\hat{\rho}\hat{a}_i^\dagger-\hat{a}_i^\dagger\hat{a}_i\hat{\rho}\right)+\text{H.c.}\Big],\end{aligned}\tag{6}$$

with $\hat{H}$ being the Hamiltonian of the coupled ring resonators with one driving coherent field

$$\begin{aligned}\hat{H} =& \sum_{k=1}^{4}\hbar\omega_k\hat{a}_k^\dagger\hat{a}_k+\mathrm{i}\hbar\big[\kappa\hat{a}_1\hat{a}_2^\dagger+\kappa\hat{a}_2\hat{a}_3^\dagger\\&+\kappa\hat{a}_3\hat{a}_4^\dagger+\epsilon\hat{a}_1\,\mathrm{e}^{\mathrm{i}\omega t}-\text{H.c.}\,\big],\end{aligned}\tag{7}$$

and the gain coefficient A and gain saturation coefficient B for the optical field within the active cavity being given by

$$A=\frac{2g^2r}{Y^2},\quad B=\frac{4g^2}{Y^2}A.\tag{8}$$

Here, g represents the coupling strength between the atoms in the gain medium and the optical field inside the active cavity, γ denotes the decay rate of the atoms and r is the pump rate of the gain medium. In the context of these expressions, it is important to note that the gain coefficient A quantifies the amplification of the optical field due to the interaction with the gain medium, while the gain saturation coefficient B describes how this amplification is affected by the intensity of the field itself. In subsequent equations, the decay rates for the cavities are specified as

$$\Gamma_1=C_1+\gamma_1,\quad \Gamma_2=C_2,\quad \Gamma_3=C_3,\quad \Gamma_4=C_4+\gamma_2,\tag{9}$$

where $C_k=\omega_k/Q_k$ $(k=1,2,3,4)$ represents the intrinsic loss rate of the ith cavity and γ_1, γ_2 account for the additional loss rates due to the coupling of the cavities to the waveguides. These decay rates are crucial for understanding the overall loss mechanisms in the system, which can significantly influence the performance and stability of the laser system.

The master equation for the field operators, given in Eq. (6), and the Hamiltonian in Eq. (7) yield the rate equations for the averaged boson operators. Namely, by using the formula

$$\frac{\mathrm{d}}{\mathrm{d}t}\langle\hat{a}_k\rangle=\mathrm{Tr}\left[\hat{a}_k\frac{\mathrm{d}}{\mathrm{d}t}\hat{\rho}\right],\quad k=1,2,3,4,\tag{10}$$

and utilizing the cyclic property of the trace operation, after substituting Eq. (6) into Eq. (10), we obtain

$$\begin{aligned}\frac{\mathrm{d}}{\mathrm{d}t}\langle\hat{a}_1\rangle =& -\mathrm{i}\omega_1\langle\hat{a}_1\rangle+\frac{G_1}{2}\langle\hat{a}_1\rangle-\kappa\langle\hat{a}_2\rangle\\&-\frac{B}{2}\left\langle\hat{a}_1^\dagger\hat{a}_1\hat{a}_1\right\rangle-\epsilon\exp\left(-\mathrm{i}\omega_1 t\right),\end{aligned}$$

$$\begin{aligned}
\frac{\mathrm{d}}{\mathrm{d}t}\langle\hat{a}_2\rangle &= -\mathrm{i}\omega_2\langle\hat{a}_2\rangle + \frac{G_2}{2}\langle\hat{a}_2\rangle - \kappa\langle\hat{a}_1\rangle \\
&\quad - \kappa\langle\hat{a}_3\rangle - \frac{B}{2}\left\langle\hat{a}_2^{\dagger}\hat{a}_2\hat{a}_2\right\rangle, \\
\frac{\mathrm{d}}{\mathrm{d}t}\langle\hat{a}_3\rangle &= -\mathrm{i}\omega_3\langle\hat{a}_3\rangle - \frac{\Gamma_3}{2}\langle\hat{a}_3\rangle - \kappa\langle\hat{a}_2\rangle - \kappa\langle\hat{a}_4\rangle, \\
\frac{\mathrm{d}}{\mathrm{d}t}\langle\hat{a}_4\rangle &= -\mathrm{i}\omega_4\langle\hat{a}_4\rangle - \frac{\Gamma_4}{2}\langle\hat{a}_4\rangle + \kappa\langle\hat{a}_3\rangle, \qquad (11)
\end{aligned}$$

where $G_i = A - \Gamma_i - \frac{7}{4}B$, $(i = 1,2)$. As one can see, the rate equations, given in Eq. (11) for the averaged quantum amplitudes, are nonlinear due to the presence of gain saturation in the active cavity. In the classical limit, i.e., in the case of large field intensities, the quantum field operators can be represented by c-number amplitudes as $\hat{a}_k \to \langle\hat{a}_k\rangle \equiv a_k$ $(k = 1,2,3,4)$. Then the rate equations in Eq. (11) can be rewritten in the classical limit as

$$\begin{aligned}
\frac{\mathrm{d}}{\mathrm{d}t}a_1 &= -\mathrm{i}\omega_1 a_1 + \frac{G_1}{2}a_1 - \kappa a_2 \\
&\quad - \frac{B}{2}|a_1|^2 a_1 - \epsilon\exp(-\mathrm{i}\omega_l t), \\
\frac{\mathrm{d}}{\mathrm{d}t}a_2 &= -\mathrm{i}\omega_2 a_2 + \frac{G_2}{2}a_2 - \kappa a_1 - \kappa a_3 - \frac{B}{2}|a_2|^2 a_2, \\
\frac{\mathrm{d}}{\mathrm{d}t}a_3 &= -\mathrm{i}\omega_3 a_3 - \frac{\Gamma_3}{2}a_3 - \kappa a_2 - \kappa a_4, \\
\frac{\mathrm{d}}{\mathrm{d}t}a_4 &= -\mathrm{i}\omega_4 a_4 - \frac{\Gamma_4}{2}a_4 - \kappa a_3. \qquad (12)
\end{aligned}$$

By substituting $a_k = A_k(t)\exp(-\mathrm{i}\omega t)$ into Eq. (12), and adjusting the parameters according to Eq. (3), one arrives at

$$\begin{aligned}
\frac{\mathrm{d}}{\mathrm{d}t}A_1 &= \mathrm{i}\Delta A_1 + 1.5\gamma A_1 - \mathrm{i}\kappa A_2 - \varepsilon - B|A_1|^2 A_1, \\
\frac{\mathrm{d}}{\mathrm{d}t}A_2 &= \mathrm{i}\Delta A_2 + 0.5\gamma A_2 - \mathrm{i}\kappa A_1 - \mathrm{i}\kappa A_3 - B|A_2|^2 A_2, \\
\frac{\mathrm{d}}{\mathrm{d}t}A_3 &= \mathrm{i}\Delta A_3 - 0.5\gamma A_3 - \mathrm{i}\kappa A_2 - \mathrm{i}\kappa A_4, \\
\frac{\mathrm{d}}{\mathrm{d}t}A_4 &= \mathrm{i}\Delta A_4 - 1.5\gamma A_4 - \mathrm{i}\kappa A_3. \qquad (13)
\end{aligned}$$

In the nonlinear scenario, the presence of multiple nonlinear terms in Eq. (13) presents a significant challenge for deriving the transmission spectrum analytically. To overcome this challenge, we have employed a numerical approach using MATLAB to solve Eq. (13) and obtain the transmission spectrum. We have set the parameters to $\epsilon = 2$ GHz, $\gamma = 1$ MHz and $B = 0.01$ Hz, and considered various coupling strengths $\kappa = 20$ MHz, 1.1 MHz and 0.1 MHz. With these settings, we were able to simulate the steady-state behavior of the system effectively. The transmission spectrum was calculated based on the ratio of the output signal to the input signal, $T(\Delta_{\mathrm{in}}) = |A_{\mathrm{out}}/A_{\mathrm{in}}|^2$, where the initial values for our numerical calculations were set to $1 \times \mathrm{e}^{-3} \times \mathrm{rand}(4,1)$. This choice of initial values, which provides a small random perturbation to the system, is crucial for the convergence of the numerical solver. We have ensured that these initial values are reasonable and consistent with the physical context of our problem. Our numerical findings indicate that the divergent peaks characteristic of the linear case transform into sharp, finite non-divergent peaks under certain parameter settings, as depicted in Figs. 3(a) and 3(d). Notably, these peaks do not exhibit non-reciprocal phenomena. In contrast, non-reciprocal transmission phenomena emerge under different parameter configurations, as shown in Figs. 3(b) and 3(e). These observations substantiate the achievement of multi-frequency non-reciprocal transmission and align with our theoretical expectations within the $\mathcal{PT}$-symmetry-breaking domain illustrated in Figs. 2(a) and 2(b). It is important to note that the parameter ϵ, representing the driving field amplitude, plays a pivotal role in the nonlinear regime. The value of ϵ has a significant influence on the strength of the nonlinear effects, and thus the emergence of non-reciprocal transmission phenomena. Our choice of $\epsilon = 2$ GHz was based on a balance between achieving noticeable nonlinear effects and maintaining the stability of the numerical simulations.

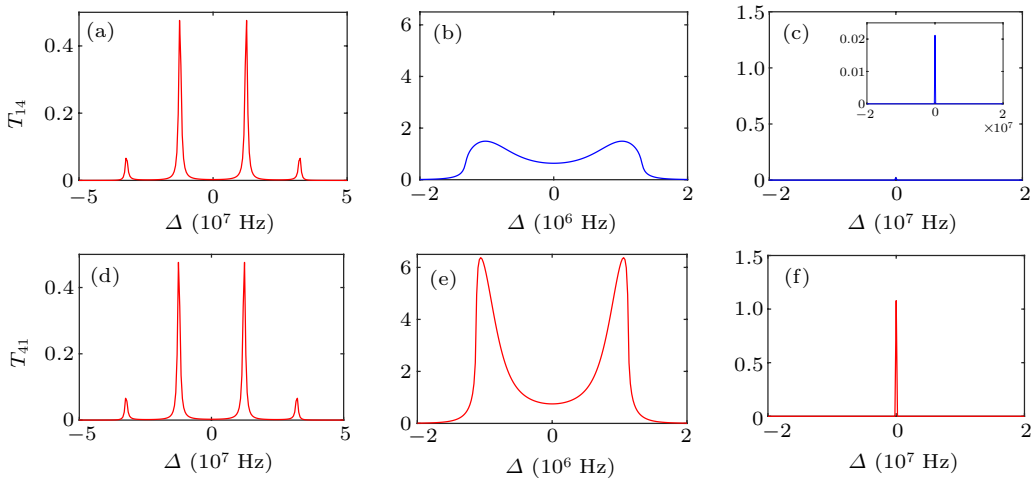


Fig. 3. Transmission spectra T_{14} and T_{41} against Δ_{in} with $\epsilon = 2$ GHz, $\gamma = 1$ MHz, $B = 0.01$ Hz: (a), (d) at $\kappa = 20$ MHz; (b), (e) at $\kappa = 1.1$ MHz; (c), (f) at $\kappa = 0.1$ MHz.

4. Construction of a dual-frequency circulator

In this section, we will introduce a nonlinear term into the original linear equation and extend a two-mode cavity system to a four-mode cavity system, in which a two-frequency non-reciprocity phenomenon can be achieved. Interestingly, the non-reciprocity of the nonlinear model can be employed to construct an optical directional amplifier simultaneously providing multi-mode optical channels with different magnifications. In other words, the non-reciprocity can provide an access to simultaneously manipulating multi-mode optical channels, which could be used in optical chip integration.

As an example, a dual-frequency non-reciprocal optical directional amplifier can be constructed by using four basic units as described in Fig. 4. Each unit consists of four ring echo wall resonators as in Fig. 1. The non-reciprocal amplifier has four ports, and any two of them can be used as signal input and output, respectively. When the signal enters the optical fiber from one of the ports it will be propagated along two routes (clockwise and counterclockwise) at the same time, as sketched in Fig. 5. Specifically, in the amplifier any port can be taken as an output to detect signals, and can be taken as an input to continue the signal execution into the next unit. The particular construction can simultaneously provide many channels for signal transmission.

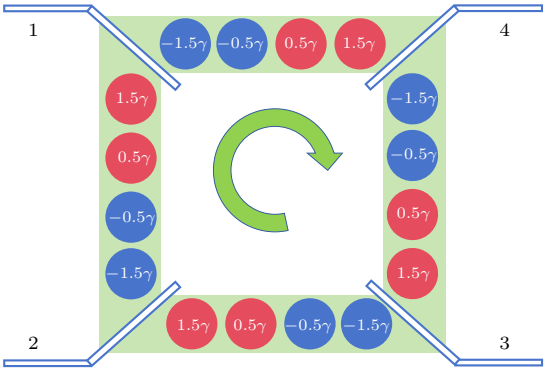


Fig. 4. Schematic diagram of multi-mode optical directional amplifier (the blue cavities are loss cavities and the red cavities are gain cavities). The device has four ports, of which any two ports can be used as signal input and output.

As can be seen from Figs. 3(b) and 3(e), when $\Delta_{\text{in}} \approx \pm 1$ MHz the basic unit exhibits extremely strong non-reciprocal behavior. This indicates that the basic unit has two non-reciprocal transmission channels with independent frequencies. Therefore, an amplifier constructed by cascading four basic units will also incorporate two parallel transmission channels with independent frequency characteristics. Moreover, signal transmission in the clockwise and counterclockwise directions demonstrates significant non-reciprocity. For the sake of simplicity, we assume that the optical signal propagates a single cycle, and we introduce a metric $\boldsymbol{M}$ to describe the transmission between the ports for the double-mode non-reciprocal amplifier. The element of metric M_{ij} $(i, j = 1,2,3,4)$ describes the transmission between the ith port and the jth port, where the ith port is input and the jth port is output. When $i = j$, the optical signal directly exits after incidence from the external fiber at the i (j) port and does not experience the amplification response of the system, so the optical signal will maintain its original state, that is, $M_{ij} = 1$ $(i = j)$. According to the non-reciprocal phenomenon of the transmission spectrum described in Figs. 3(b) and 3(e), combined with Figs. 5 and 4, it can be inferred that the optical signal incident from the ith port and the effect of four cascade structures will be superimposed, and the maximum output signal will be detected at the $j = i+1$-th port (specifically, when $i = 4$, $j = 1$). For example, we can describe the transmission from port 1 to port 2 as $M_{12} = T_{41}^3 + T_{14}$, where T_{14} and T_{41} represent the transmission of the basic unit as shown in Figs. 3(b) and 3(e). By calculation, we obtain that M_{12} is about 254. In the same way, we can obtain $M_{23} = M_{34} = M_{41} = T_{41}^3 + T_{14} = 254$.

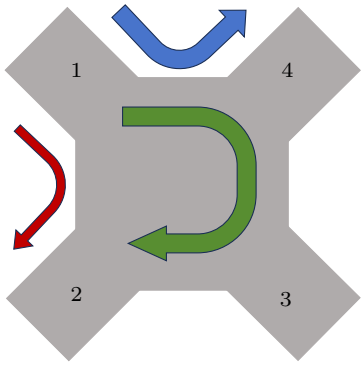


Fig. 5. Schematic diagram of an optical nonreciprocal directional amplifier. When the signal light is routed in a clockwise direction, as shown by the blue arrow, there is a large amplification factor between ports. When the signal light is routed in a counterclockwise direction, as shown by the red arrow, there is a small amplification factor between ports. The green arrow represents our ideal signal routing direction.

In order to better characterize the performance of the optical non-reciprocal directional amplifier, the amplification coefficient matrix in the ideal case is given as shown in Fig. 6(a), where M_{ij} $(i = 1,2,3,4,\ j = i+1)$ is so much larger than M_{ij} $(i = 1,2,3,4,\ j \neq i+1)$ that the latter is negligible. In fact, we calculate $M_{13} = T_{41}^2 + T_{14}^2$, $M_{14} = T_{41} + T_{14}^3$ and other ports. The amplification factor of the amplifier mentioned above is dependent on frequency. To characterize this frequency dependence, three-dimensional views of the amplification coefficient matrices are presented in Figs. 6(b), 6(c) and 6(d) for frequency detunings $\Delta_{\text{in}} = \pm 1.04$ MHz, $\Delta_{\text{in}} = \pm 0.9$ MHz and $\Delta_{\text{in}} = \pm 1.12$ MHz, respectively. From these visualizations, it is evident that within at least the range of ± 0.9 MHz to ± 1.12 MHz, the directional amplifier system exhibits pronounced non-reciprocal behavior, enabling multistage amplification. The results may provide a way for the non-reciprocal amplifier to be included in complex opto-mechanical structures and implemented in integrated photonic circuits.

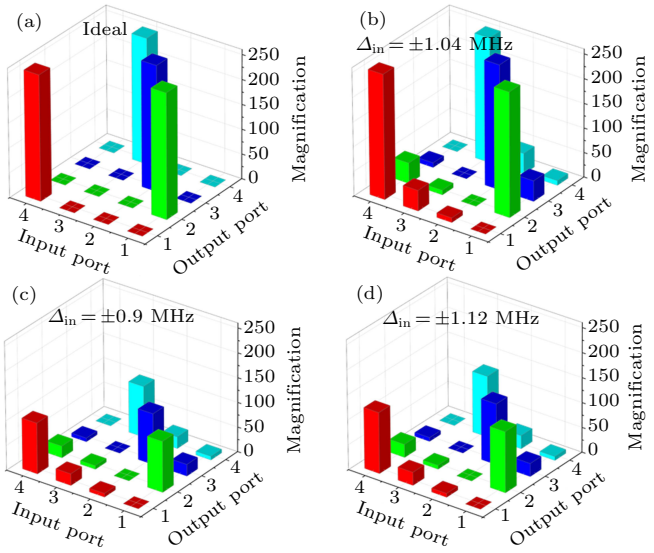


Fig. 6. Amplification coefficient matrix of the multi-mode optical directional amplifier for a single cycle. (a) The ideal magnification matrix. $M_{12} = M_{23} = M_{34} = M_{41} = 254$. (b)–(d) The numerically simulated magnification matrix for frequency detunings $\Delta_{in} = \pm 1.04$ MHz, $\Delta_{in} = \pm 0.9$ MHz and $\Delta_{in} = \pm 1.12$ MHz, respectively. i and j are, respectively, input ports and output ports, and the optical signal will be continuously amplified in the clockwise direction. The special case is $M_{ij} = 1$ $(i = j)$.

5. Conclusion

In summary, based on the Scully–Lamb model and photomechanical interaction, we have constructed a non-reciprocal unit that is a system coupled by four resonators and two optical fibers. In the constructed system the transmission rate has different values in a particular direction and its opposite one. Due to the presence of many ports and simultaneously distinguishable transmission rates in the non-reciprocal unit, the dual-frequency non-reciprocity phenomenon can realize parallel transmission and processing of information. Further, it can be integrated into photonic circuits or optical devices.[37,38,48] As communication applications, one can construct optical isolators, circulators and directional amplifiers[41,44–46] that can be used to control optical signals in a particular direction at specific frequencies. For magneto-optical storage, one can design magneto-optical materials and devices[49] with the non-reciprocal units.

For an example, a multi-mode optical directional amplifier with four ports was archived using the basic units. For a particular input port the other three output ports can have distinguishable amplification times of optical signals, resulting from their non-reciprocity. These results may provide a solution for the more and more complex requirements for the signals in communication and optical integrated circuits. Moreover, our example can be arbitrarily extended to more ports that can be integrated on a chip with other circuit components in barrier-free combination.

Appendix A: Derivation of non-linear coupled differential equations

The gain saturation effect is a pivotal phenomenon in laser physics in which the intensity of the intracavity field becomes significant enough to reduce the net gain of the active medium. As the Scully–Lamb quantum laser model is applied to parity–time symmetric whispering-gallery microcavities, the gain saturation effect plays an important role in explaining non-reciprocity in light propagation. When the intensity of the input driving field increases, the gain ability of medium will diminish due to saturation, which equivalently decreases the amplification of the signal field. This nonlinear mechanism results in a direction-dependent transmission behavior which is essential for non-reciprocal light transmission in the broken $\mathcal{PT}$-symmetric phase. The model demonstrates that gain saturation modifies the eigenmodes and exceptional points of the system by introducing an additional loss mechanism that depends on the field intensity and direction of propagation. In Ref. [5], the authors employ the Scully–Lamb quantum laser model to derive a set of rate equations that describe the dynamics of light propagation in parity–time symmetric whispering-gallery microcavities. Starting from a non-Lindbladian master equation that accounts for gain, loss and gain saturation, they apply the semiclassical approximation to transform quantum operators into classical amplitudes. By calculating the time derivatives of these amplitudes and incorporating the effects of gain saturation, at a set of nonlinear coupled differential equations are obtained that can elucidate the interplay between the intracavity fields and the response of the photonic system and reveal the nonreciprocal transmission of light. This theoretical framework bridges the quantum and classical descriptions and provides a way to learn about the action of gain saturation on non-reciprocal behavior.

One of the simplest examples is a two-mode array with balanced gain and loss, as shown in Fig. A1(a). This system can be easily built from the general structure as shown in Fig. 1 and Eq. (1) by setting $N = 2, \gamma_1 = \gamma, \gamma_2 = -\gamma$ and $\kappa_{1,2} = \kappa_{2,1} = \kappa$, where we have assumed $\gamma, \kappa > 0$. Repeating the progress of Eqs. (1)–(5), we can get the evolution matrix of the two-mode array:

$$\hat{\boldsymbol{H}}_2 = \begin{pmatrix} \Delta_{in} + i\gamma & \kappa \\ \kappa & \Delta_{in} - i\gamma \end{pmatrix}. \tag{A1}$$

According to Eq. (4), the transmission spectrum can be given by

$$T(\Delta_{in}) = \left|\frac{A_{out}}{A_{in}}\right|^2 = \left|\frac{A_2}{\epsilon}\right|^2 \gamma_c^2, \tag{A2}$$

where A_2 can be solved by $\boldsymbol{\alpha} = \boldsymbol{\beta}\hat{\boldsymbol{H}}_2^{-1}$, wherein $\boldsymbol{\alpha} = (A_1, A_2)^T$, $\boldsymbol{\beta} = (\epsilon, 0)^T$. In the complex plane, the distribution of supermodes as γ/κ vary across the EP as shown in

Fig. A1(d). When $\gamma/\kappa < 1$, the supermodes $\Delta_\pm$ lie on the real axis denoted by blue rhomboid. In this region, the transmission spectrum diverges at these points described in Fig. A1(e). When $\gamma/\kappa > 1$, the values of $\Delta_\pm$ become purely imaginary as the red cross in Fig. A1(d). Since the input detuning $\Delta_{\rm in}$ is always a real number, the divergent peaks vanish in the transmission spectrum, and are replaced by a broad finite peak at $\Delta_{\rm in} = 0$ which is the projection of $\Delta_\pm$ on the real axis, as shown in Fig. A1(f). In fact, according to $T(\Delta_{\rm in}) = |\kappa\gamma_{\rm c}/(\Delta_{\rm in}^2 + \gamma^2 - \kappa^2)|^2$, it is easy to check that the spectrum can fits the square of a Breit–Wigner distribution around $\Delta_{\rm in} = 0$ when $\gamma^2 - \kappa^2 > 0$. The peaks are called Breit–Wigner peaks.[50]

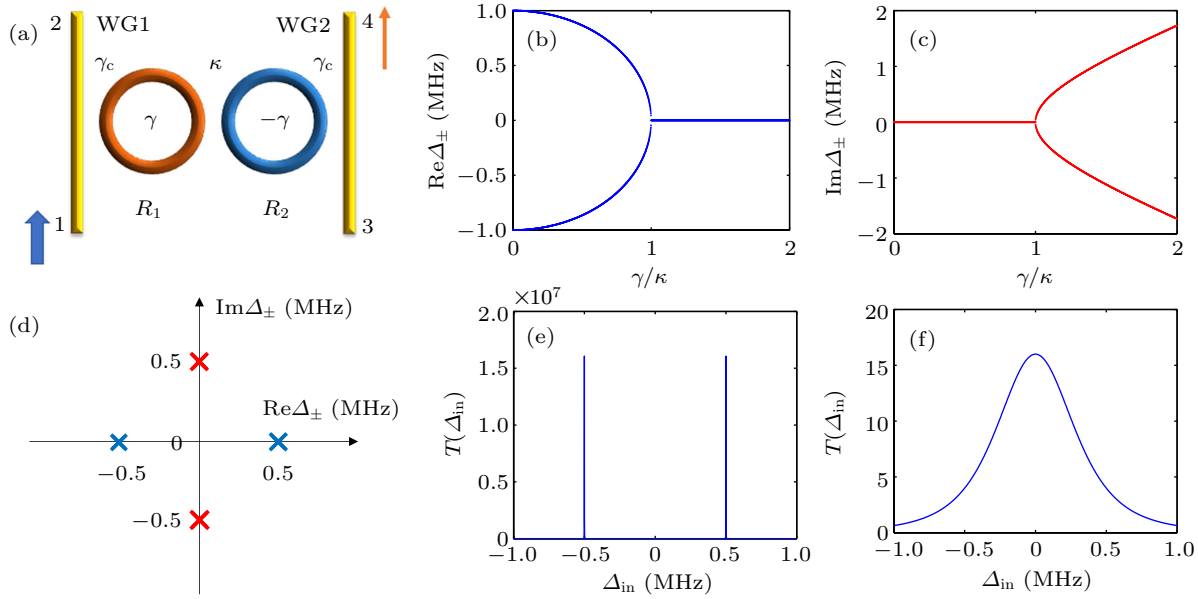


Fig. A1. (a) The sketch of the two-mode $\mathcal{PT}$ symmetric system, wherein balanced gain (loss) is labeled by γ ($-\gamma$), coupling between the two resonators is κ, and $\gamma_{\rm c}$ denotes the couplings between the resonator (R_1 and R_2) and the waveguide (WG1 and WG2). (b) The real part of supermodes $\Delta_\pm$ of $\hat{H}_2$ as a function of γ/κ with $\kappa > 0$. (c) The imaginary part of $\Delta_\pm$ of $\hat{H}_2$ as a function of γ/κ with $\kappa > 0$. (d) The distribution of supermodes $\Delta_\pm$ on the complex plane where $\kappa = 1$ MHz. Blue rhomboid corresponds to $\mathcal{PT}$ unbroken region ($\gamma = \sqrt{3}/2$ MHz). Red cross corresponds to $\mathcal{PT}$ broken region ($\gamma = \sqrt{5}/2$ MHz). (e), (f) Transmission spectrum against input frequency $\Delta_{\rm in}$ in the $\mathcal{PT}$ unbroken ((e), $\gamma = \sqrt{3}/2$ MHz) and broken ((f), $\gamma = \sqrt{5}/2$ MHz) regions, wherein $\kappa = \gamma_{\rm c} = 1$ MHz, $\epsilon = 0.1$ MHz.

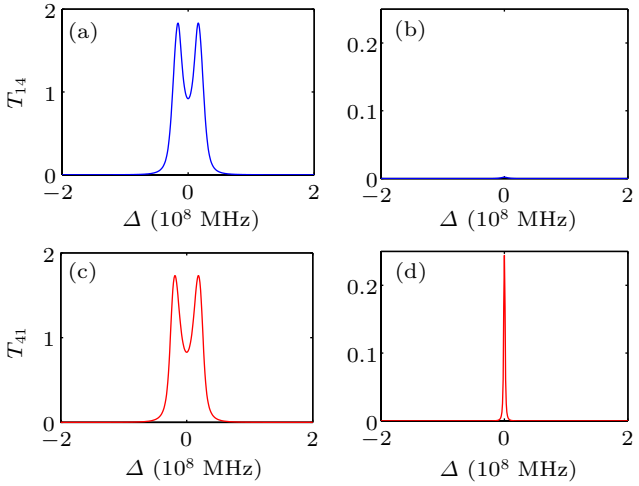


Fig. A2. Transmission spectrum T_{14} and T_{14} against $\Delta_{\rm in}$ wherein $\epsilon = 176.05$ GHz, $B = 0.01$ Hz, (a), (c) $\gamma = 3.766$ MHz, $\kappa = 20$ MHz, (b), (e) $\gamma = 3.766$ MHz, $\kappa = 0.2$ MHz.

By considering the gain saturation effect, the linear equation can be reformulated into the following nonlinear form:

$$\begin{aligned}\frac{\rm d}{{\rm d}t}A_1 &= {\rm i}\Delta A_1 + \gamma A_1 - \kappa A_2 - \frac{B}{2}|A_1|^2 A_1 - \epsilon,\\ \frac{\rm d}{{\rm d}t}A_2 &= {\rm i}\Delta A_2 - \gamma A_2 + \kappa A_1.\end{aligned} \tag{A3}$$

Comparing Eqs. (13) and (A3), it can be seen that the nonlinear equation includes an additional cubic term. When the optical field inside the resonator is weak, that is A_1 being small, this term can be negligible due to the coefficient B being very small. However, when the optical field increases, that is A_1 becoming larger, the cubic term increases dramatically, causing a substantial suppression of the field intensity, thus the field intensity cannot be linearly enhanced without limit.

Then we can calculate the transparency spectrum using this model, as shown in Fig. A2. When γ is small, which corresponds to the $\mathcal{PT}$-symmetric unbroken phase depicted in Fig. A1(e), the original divergent peaks are constrained and transforms into non-divergent peaks, and exhibit reciprocity as shown in Figs. A2(a) and A2(c). Conversely, when γ is large, corresponding to the $\mathcal{PT}$-symmetric broken phase shown in Fig. A1(f), the position of the original divergent peak remains unchanged, but the peak value of T_{41} is significantly larger than that of T_{14}, demonstrating non-reciprocity, as shown in Figs. A2(b) and A2(d). This agrees with the experimental results reported in Ref. [6].

Acknowledgments

This work is jointly supported by the National Nature Science Foundation of China (Grant Nos. 12475019 and 12073056), the Major National Science and Technology Project of China (Grant No. BX2024B054), National Lab of Solid State Microstructure of Nanjing University (Grant Nos. M35040, M35053, and M37014), and the Natural Science Foundation of Shandong Province (Grant No. ZR2024MA038).

References

[1] Meng H, Ang Y S and Lee C H 2024 *Appl. Phys. Lett.* **124** 060502
[2] Yan Q, Zhao B, Zhou R, Ma R, Lyu Q, Chu S, Hu X and Gong Q 2023 *Nanophotonics* **12** 2247
[3] Shen Z, Zhang Y L, Chen Y, Sun F W, Zou X B, Guo G C, Zou C L and Dong C H 2018 *Nat. Commun.* **9** 1
[4] Andreas R, Miguel A S, Anthony K and Muga J G 2021 *J. Phys. Conf. Ser.* **2038** 012020
[5] Arkhipov I I, Miranowicz A, Di Stefano O, Stassi R, Savasta S, Nori F and Özdemir K 2019 *Phys. Rev. A* **99** 053806
[6] Chang L, Jiang X, Hua S, Yang C, Wen J, Jiang L, Li G, Wang G and Xiao M 2014 *Nat. Photonics* **8** 524
[7] Potton R J 2004 *Rep. Prog. Phys.* **67** 717
[8] Shen Z, Zhang Y L, Chen Y, Xiao Y F, Zou C L, Guo G C and Dong C H 2023 *Phys. Rev. Lett.* **130** 013601
[9] Kutsaev S V, Krasnok A, Romanenko S N, Smirnov A Y, Taletski K and Yakovlev V P 2021 *Adv. Photonics Res.* **2** 2000104
[10] Bromberg Y, Redding B, Popoff S M and Cao H 2016 *Phys. Rev. A* **93** 023826
[11] Zheng J C and Li P B 2023 *Opt. Express* **31** 21881
[12] Fan Z, Zhang W, Qiu Q and Yao J 2020 *J. Lightwave Technol.* **38** 2127
[13] Mock A 2022 *Opt. Express* **30** 39207
[14] Cheng S, Shen H Z and Yi X X 2019 *Opt. Express* **27** 25882
[15] Tang L, Tang J, Chen M, Nori F, Xiao M and Xia K 2022 *Phys. Rev. Lett.* **128** 083604
[16] Yao Y and Ai Q 2023 *Ann. Phys.* **535** 2300135
[17] Burgwal R and Verhagen E 2023 *Nat. Commun.* **14** 1526
[18] Cao W, Wang C, Chen W, Hu S, Wang H, Yang L and Zhang X 2022 *Nat. Nanotechnol.* **17** 262
[19] Liao M J, Wei M S, Wang S, Xu J and Yang Y 2024 *Chin. Phys. B* **33** 060305
[20] Yi Y 2024 *Chin. Phys. B* **33** 060302
[21] Metelmann A and Clerk A A 2017 *Phys. Rev. A* **95** 013837
[22] Shoji Y and Mizumoto T 2016 *Sci. Technol. Adv. Mater.* **15** 014602
[23] Yan W, Wei Z, Yang Y, Wu D, Zhang Z, Song X, Qin J and Bi L 2024 *Optica* **11** 376
[24] Hu X X, Wang Z B, Zhang P, Chen G J, Zhang Y L, Li G, Zou X B, Zhang T, Tang H X, Dong C H, Guo G C and Zou C L 2021 *Nat. Commun.* **12** 2389
[25] Caloz C, Alù A, Tretyakov S, Sounas D, Achouri K and Deck-Léger Z L 2018 *Phys. Rev. Appl* **10** 047001
[26] Caloz C and Deck-Léger Z L 2019 *T-AP* **68** 1569
[27] Sounas D L and Alù A 2017 *Nat. Photonics* **11** 774
[28] Fan S, Shi Y and Lin Q 2018 *AWP Letters* **17** 1948
[29] Estep N A, Sounas D L, Soric J and Alù A 2014 *Nat. Phys.* **10** 923
[30] Fang K, Yu Z and Fan S 2012 *Nat. Photonics* **6** 782
[31] Tzuang L D, Fang K, Nussenzveig P, Fan S and Lipson M 2014 *Nat. Photonics* **8** 701
[32] Lira H, Yu Z, Fan S and Lipson M 2012 *Phys. Rev. Lett.* **109** 033901
[33] Fang K, Yu Z and Fan S 2012 *Phys. Rev. Lett.* **108** 153901
[34] Fan L, Varghese L T, Xuan Y, Wang J, Niu B and Qi M 2012 *Opt. Express* **20** 20564
[35] Guo X, Zou C L, Jung H and Tang H X 2016 *Phys. Rev. Lett.* **117** 123902
[36] Lawrence M, Barton D R and Dionne J A 2018 *Nano Lett.* **18** 1104
[37] Peterson G, Lecocq F, Cicak K, Simmonds R, Aumentado J and Teufel J 2017 *Phys. Rev. X* **7** 031001
[38] Barzanjeh S, Wulf M, Peruzzo M, Kalaee M, Dieterle P B, Painter O and Fink J M 2017 *Nat. Commun.* **8** 953
[39] Bernier N R, Tóth L D, Koottandavida A, Ioannou M A, Malz D, Nunnenkamp A, Feofanov A K and Kippenberg T J 2017 *Nat. Commun.* **8** 604
[40] Mercier de Lépinay L, Ockeloen-Korppi C F, Malz D and Sillanpää M A 2020 *Phys. Rev. Lett.* **125** 023603
[41] Malz D, Tóth L D, Bernier N R, Feofanov A K, Kippenberg T J and Nunnenkamp A 2018 *Phys. Rev. Lett.* **120** 023601
[42] Peng B, Özdemir K, Lei F, Monifi F, Gianfreda M, Long G L, Fan S, Nori F, Bender C M and Yang L 2014 *Nat. Phys.* **10** 394
[43] Du C, Chen Y T, Du L and Wu J H 2024 *Phys. Lett. A* **503** 129413
[44] Bi L, Hu J, Jiang P, Kim D H, Dionne G F, Kimerling L C and Ross C A 2011 *Nat. Photonics* **5** 758
[45] Wu H, Tang J, Chen M, Xiao M, Lu Y, Xia K and Nori F 2024 *Opt. Express* **32** 11010
[46] Shen J, Liu J, Lin M, Wu Z and Deng S 2023 *Electron. Lett.* **59** e212730
[47] Yamamoto Y and Imamoglu A 1999 *Mesoscopic Quantum Optics* (New York: John Wiley & Sons)
[48] Dong C, Yang Z, Zeng J and Hu J 2023 *Chin. Phys. B* **32** 070305
[49] Cotrufo M, Cordaro A, Sounas D L, Polman A and Alù A 2023 *Nat. Photonics* **18** 81
[50] Breit G and Wigner E 1936 *Phys. Rev.* **49** 519